

Performance evaluation of add drop filter by studying rod shape and filling fraction

S. ROBINSON*, NAKKEERAN

Department of Electronics and Communication Engineering, Pondicherry Engineering College, Pondicherry-605014, India

The impacts of rod shape and filling fraction are studied for the Two Dimensional (2D) circular Photonic Crystal Ring Resonator (PCRR) based Add Drop Filter (ADF). The ADFs are devised separately using rods of square, circular and hexagonal shape in square lattice PC. For various values of rod's cross sectional dimension and shape the resonant wavelength, coupling efficiency, dropping efficiency, Q factor and passband width of the designed filters are carried out through simulation. The calculated filling fraction of a square, circular and hexagonal rods in the lattice structure is 0.04×10^{-12} sq.m, 0.0314×10^{-12} sq.m and 0.0346×10^{-12} sq.m and their respective resonant wavelength is 1523 nm, 1497 nm and 1507 nm. It is observed that there is 1 nm wavelength shift to longer wavelength while increasing the overall filling fraction by 0.1233×10^{-12} sq.m. Here, the 2D Finite Difference Time Domain (FDTD) method and Plane Wave Expansion (PWE) method are employed for obtaining the normalized transmission and band diagram of the PC structure.

(Received August 22, 2011; accepted September 15, 2011)

Keywords: Photonic crystal, Circular ring resonator, Photonic band gap, Add drop filter, FDTD method, PWE method, Square rods, Circular rods, Hexagonal rods

1. Introduction

After the invention of Photonic Crystal (PC) by E. Yablonovitch [1] and S. John [2] in 1987, Two Dimensional (2D) PC has gained tremendous research across the globe in the past two decades owing to huge potential for integration in Photonic Integrated Circuits (PIC). PCs can offer very high speed of operation, tolerance to temperature fluctuation, increased life time, flexible design, ultra compact size with ease integration capability, excellent performance, and able to realize in different materials and shapes depending upon the applications. The selection of rod shape to design the optical device and performance variation owing to the rod shape is essential to study. The performance is examined by considering PC based Add Drop Filter (ADF).

Typically, ADF is one of the prominent components for telecommunication, short haul, enterprise and metro access optical networks to drop a particular channel without disturbing other channels departing through the fiber or to select a required channel and remove all other channels. Conventional ADFs are proposed and realized by Fabry-Perot filter, thin film filter, arrayed waveguide grating based filter, bragg grating based filter, acousto and electro optic filter, and micro ring resonator based filter [3]. Among them, micro ring resonator based ADF provides significant performance as it has high spectral selectivity, wide tunability, flexible mode design and reduced channel spacing. The selectivity can be varied by varying the radius or size of the ring resonator and the material used for the structure. In conventional MicroElectroMechanical Systems (MEMS) based ADFs, when the radius of the ring resonator is reduced below 5

μm , the propagation and bending losses become significant and increase thereafter. On the other hand, the Photonic Crystal (PC) based Ring Resonator (RR) can overcome the aforementioned bottleneck and help the designer to design a device in the order of micrometers with the improved performance.

Generally, PCs are composed of periodic dielectric and metallo-dielectric nanostructures that have alternate low and high dielectric constant materials (refractive index) in one, two and three dimensions, which affect the propagation of electromagnetic waves inside the structure. As a result of this periodicity, it possesses Photonic Band Gap (PBG) where the propagation of light is completely prohibited for certain frequency ranges. By introducing defects (point or line) in these periodic structures, the band gaps are disturbed and the light propagation can be made possible in the PBG region. This leads to the design of PC based optical devices (active and passive) in the PBG region [4, 5].

Recent years, many pillar type PC based optical devices are proposed and designed such as power splitters [6], multiplexers [7], demultiplexers [8], polarization beam splitters [9], triplexers [10], switches [11], directional couplers [12], bandstop filters [13], bandpass filters [14,15], channel drop filters [16-19], add-drop filters [20-23], etc. The above said PC based optical devices are designed and realized in square and triangular lattice using square, circular and hexagonal rods. However, so far, there is no attempt has been made to study the impact of a device by using different rod shapes. It is witnessed that the pillar type circular Photonic Crystal Ring Resonator (PCRR) offers substantial performance [24] than square, quasi square, dual quasi square and hexagonal PCRRs.

Hence, the circular PCRR based ADF with different rod shapes is considered here for further study of filling fraction.

In this paper, an attempt is made to study the impact of rod shape and filling fraction by designing and comparing the performance of Two Dimensional (2D) circular Photonic Crystal Ring Resonator (PCRR) based ADF. The resonant wavelength, coupling efficiency, dropping efficiency, Q factor and passband width are investigated with and without using scatterer rods. Filtering response is obtained using Finite Difference Time Domain (FDTD) method and Plane Wave Expansion (PWE) method is used to calculate the propagation modes and band gap of periodic and non periodic structures.

The remaining part of this paper is arranged as follows: In Section 2, the structure design and its band diagram and filling fraction of square, circular and hexagonal rods based structure is described in detail. The PCRR based ADFs and their simulation results are discussed in Section 3 and Section 4. Finally, Section 5 concludes the paper.

2. Structure design and calculation of filling fraction

The proposed ADF with different rod shapes is designed using two dimensional square lattice PC. The number of rods positioned in 'X' and 'Z' directions are 21. The distance between the two adjacent rods is 540 nm which is termed as lattice constant 'a'. The radius (r) of the rod is 0.1 μm and the Silicon (Si) rod with refractive index 3.46 is positioned in air host.

Fig. 1 shows the schematic structure of designed ADF without scatterer rods. The values (radius of the rod, lattice constant and refractive index) considered for designing the ADF are optimized through gap map. It gives the value to design the device with respect to TE/TM (Transverse Electric/Transverse Magnetic) PBG. The gap maps for square, circular and hexagonal rods are described in detail in the Appendix. The Perfect Matched Layer (PML) is placed as absorbing boundary condition [25].

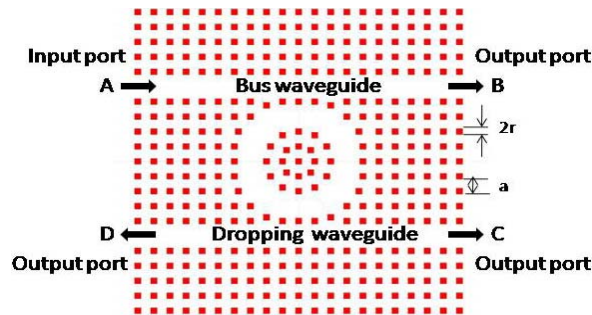


Fig. 1. Schematic structure of PCRR based ADF using square rods without scatterer rods.

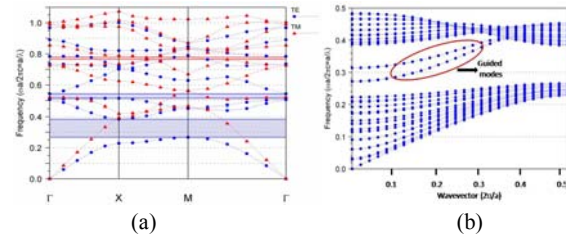


Fig. 2. Band diagram of square rods in square lattice structure (a) without introducing any defects (1×1 PC-unit cell) (b) after the introduction of defects (21×21 PC-super cell).

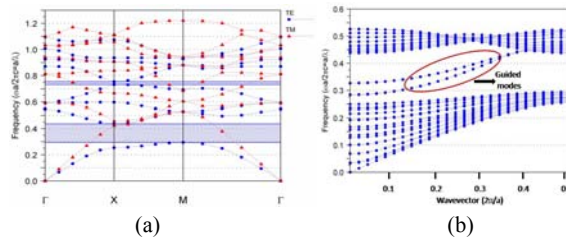


Fig. 3. Band diagram of circular rods in square lattice structure (a) without introducing any defects (1×1 PC-unit cell) (b) after the introduction of defects (21×21 PC-super cell).

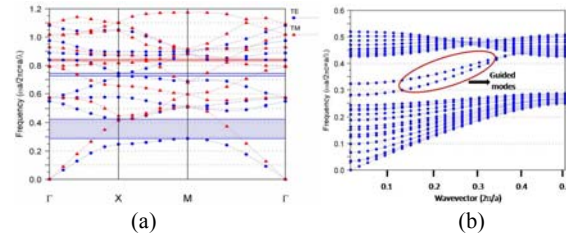


Fig. 4. Band diagram of hexagonal rods in square lattice structure (a) without introducing any defects (1×1 PC-unit cell) (b) after the introduction of defects (21×21 PC-super cell).

The band diagram shown in Figs. 2 (a), 3 (a) and 4 (a) give the propagation modes and TE/TM PBG present in the 1×1 PC structure of square, circular and hexagonal rods in the square lattice structure, respectively. They have (both) TE and TM PBG. Here the first reduced TE PBG is considered for designing the ADF for third window of optical communication whose electric field is parallel to the rod axis. The TE/TM PBGs with normalized frequencies and their corresponding wavelength range for square, circular and hexagonal rods are listed in Table 1 where the data in bold represents that the ranges of first TE PBG.

Table 1. Frequency and wavelength range of TE/TM PBG of circular, hexagonal and square rods.

Rod Shape	PBG	Frequency (a/λ)	Wavelength Range (nm)
Square rods	TE	0.2675-0.384 0.5122-0.5415	1406-2018 997-1054
	TM	0.7645-0.778	694-706
Circular rods	TE	0.295-0.436 0.7245-0.745	1238-1830 724-745
Hexagonal rods	TE	0.2875-0.4245 0.7245-0.745	1272-1878 724-745
	TM	0.8315-0.8435	640-649

The band diagram after the introduction of line and point defects (21×21 PC) with square, circular and hexagonal rods is clearly pictured in Figs. 2 (b), 3 (b) and 4 (b), respectively. It is observed that, the TE PBG has been entirely distributed and the guided modes propagate inside this PBG region.

The number of rods used in ‘X’ and ‘Z’ directions is 21 which determines the filling factor in turn the foot print of the ADF using different rod shape is same. The filling factor is the number of rods placed in the structure. The filling fraction is defined as the space occupied by rods in a lattice which is nothing but the area covered by rods in a lattice. Since, we have considered square, circular and hexagonal rods, the area of single rod and entire rods are calculated primarily by using the basic formulae of the respective geometry.

The value of area (a), radius (r) and width (w) for square, circular and hexagonal rods are 0.2 μm, 0.1 μm and 0.2 μm, respectively. The calculated filling fraction of single rod and entire rods in the structure after the introduction of the defects and other details are listed in the Table 2.

Table 2. Calculated filling fraction of single and total number of rods in a lattice.

Rod shape	Area of single rod (sq.m)	Area after the introduction of defects (sq.m)	Area of square lattice (sq.m)
Square rods	0.04×10^{-12}	15×10^{-12}	129.96×10^{-12}
Circular rods	0.0314×10^{-12}	11.775×10^{-12}	129.96×10^{-12}
Hexagonal rods	0.0346×10^{-12}	12.975×10^{-12}	129.96×10^{-12}

The table shows the filling fraction of square rod is higher which results the resonance to occur at longer wavelength whereas circular rod has low filling fraction in turn lower resonant wavelength. The total number of rods in a structure is (21×2)1441 and the rods that are removed for the defects are 66 hence the total number of rods in a structure after the introduction of line and point defects becomes 375. The area of single rod is calculated and then

that is multiplied by 375 to get the overall filling fraction of the structure.

A linear relationship is observed between the resonant wavelength and filling fraction irrespective of the shape of the rod and also while varying the cross sectional dimension of the rod.

3. Photonic crystal ring resonator based ADF

In general, a ring resonator is positioned between two optical waveguides to provide an ideal basic structure for ADF. The power in one waveguide is coupled into the other through ring resonator at resonance. Fig. 5 shows the schematic structure of ADF, which consists of bus and dropping waveguides and ring resonator (coupling element). Also, it has four ports, ports 1 and 2 are the input and transmission output terminals whereas ports 3 and 4 are forward and backward dropping terminals, respectively.

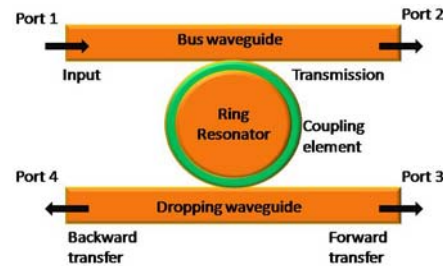


Fig. 5. Schematic structure of ADF.

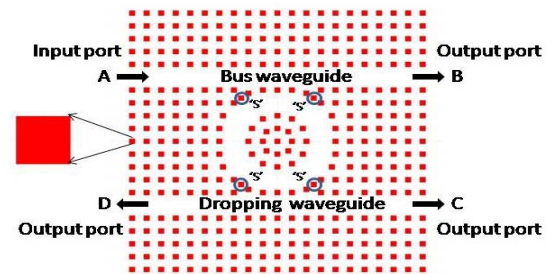


Fig. 6. Schematic structure of PCRR based ADF using square rods with scatterer rods.

Fig. 6 depicts PCRR based ADF using square rods with scatterer rods and Figs. 7 (a) and (b) present the ADF based on circular and hexagonal rods with scatterer rods, respectively. They consist of two waveguides in horizontal (r-x) direction and a circular PCRR is placed between them. The top waveguide is called as bus waveguide whereas bottom waveguide is termed as dropping waveguide.

The input signal port is marked ‘A’ with arrow in the top (bus) waveguide. The ports ‘C’ and ‘D’ of bottom (drop) waveguide are the drop terminals and denoted as forward dropping and backward dropping terminals, respectively, while the port ‘B’ of the top waveguide is defined as the forward transmission terminal. The bus

waveguide is formed by introducing line defects which is done by either removing or changing the shape or size of the rods in rows or columns in uniform direction and the circular PCRR is shaped by point defects (i.e. by removing or changing the columns or rows of rods in non-uniform direction to make a circular shape).

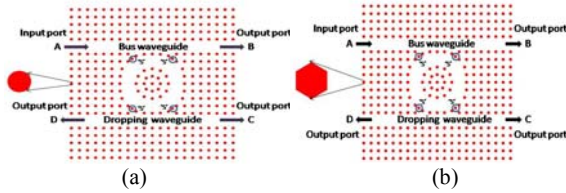


Fig. 7. Schematic structure of circular PCRR based ADF with scatterer rods with (a) circular rods and (b) hexagonal rods.

The PCRR is constructed by varying the position of inner rods and outer rods from its original position towards center. The inner rods are built by varying the position of adjacent rods in the four sides, from its center, by 25%, whereas the outer rods are constructed by varying the position of second rod in the four sides, from its center, by 25% in both 'X' and 'Z' directions where 'X' is the horizontal direction and 'Z' is the vertical direction. The number of rings that is formed by the inner rod is three. The position of the rods is varied by varying the lattice constant. The rods which are inside the circular PCRR is called as inner rods whereas the coupling rods which are placed between circular PCRR and waveguides.

The scatterer rod ('s') is placed in each corner of the ring resonator with half lattice constant which is used to enhance the performance of the ADF by reducing the counter propagation modes at resonance and off resonance. The material properties, size and shape of the scatterer rods are similar to other rods. At resonance, the wavelength is coupled into the dropping waveguide from bus waveguide and exits through one of the output ports. The coupling and dropping efficiencies are noted by monitoring the power at ports 'B' and 'C' & 'D', respectively. To maximize the output power efficiency, the cavity has to support two degenerate modes with odd and even symmetry with respect to an axis orthogonal to the waveguides [26]. The designed structure has two degenerate modes as shown in Figs. 2 (b), 3 (b) and 4 (b).

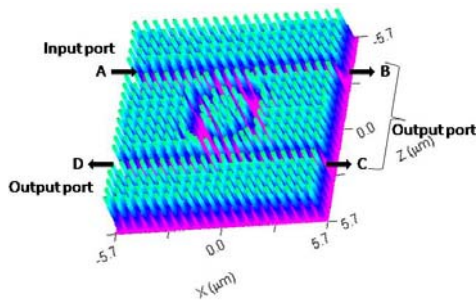


Fig. 8. Three dimensional view of circular PCRR based ADF.

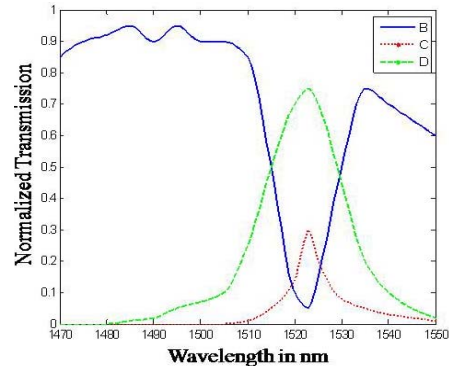
The three dimensional view of PCRR based ADF is shown in Fig. 8. It illustrates that the arrangement of Si rods in a structure and the overall size of the device is $11.4 \mu\text{m} \times 11.4 \mu\text{m}$.

4. Simulation results

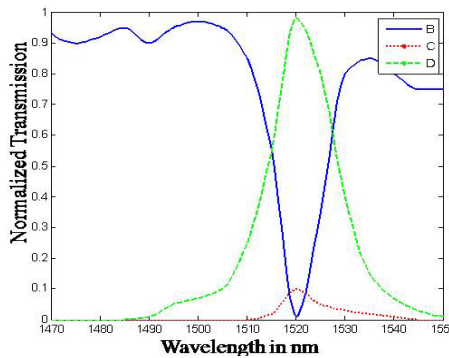
A Gaussian input signal is launched into the input port. The normalized transmission spectra are obtained at ports 'B', 'C' and 'D' by conducting Fast Fourier Transform (FFT) of the fields that are calculated by 2D FDTD method. The input and output signal power is recorded by power monitors which are positioned at the input and output ports. The normalized transmission is calculated through the following formula

$$T(f) = \frac{1/2 \int \text{real}(p(f)^{\text{monitor}}) \cdot dS}{\text{SourcePower}} \quad (12)$$

Where $T(f)$ is a normalized transmission as a function of frequency, $p(f)$ is a poynting vector and dS is the surface normal. The further normalization at the output side does not affect the result because of the source power normalization.

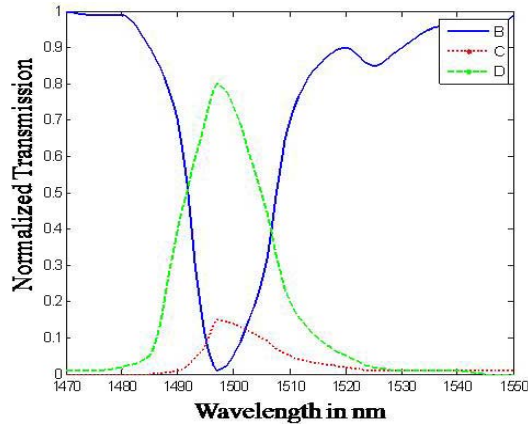


(a)

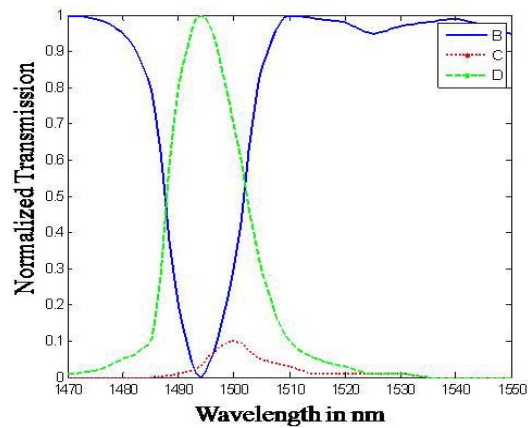


(b)

Fig. 9. Normalised transmission spectra of square rod PCRR based ADF (a) without and (b) with scatterer rods.



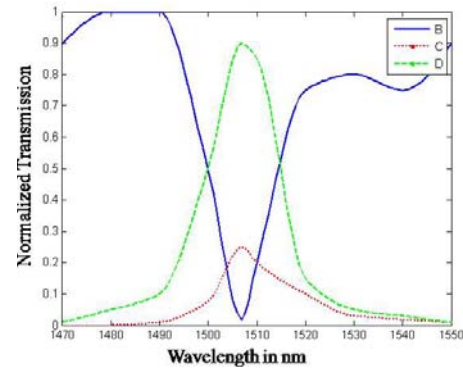
(a)



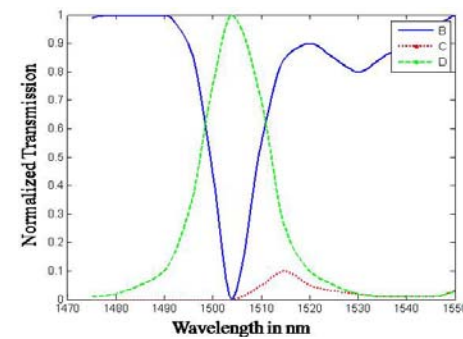
(b)

Fig. 10. Normalised transmission spectra of circular rod PCRR based ADF (a) without and (b) with scatterer rods.

Figs. 9 (a) and (b) show the normalized transmission spectra of square rods based ADF without and with scatterer rods. Similarly the normalized transmission spectra of circular and hexagonal rods based ADF without and with scatterer rods are shown in Figs. 10 (a) and (b), and Figs. 11 (a) and (b), respectively. The response of the result have clearly shown that circular and hexagonal rod shape with scatterer rods provide 100% coupling and dropping efficiencies and their Q factor is 124.5 and 107.4, respectively, which are meeting the requirements for ITU-T G. 694.2 eight channel Coarse Wavelength Division Multiplexing (CWDM) system [27]. It is also observed that the output power at port 'C' is nullified by inserting the scatterer rods which successively enhance the output efficiency at resonance and beyond the resonance as well.



(a)



(b)

Fig. 11. Normalised transmission spectra of hexagonal rod PCRR based ADF (a) without and (b) with scatterer rods.

Although, shape, size of the ring resonator and number of rods in the considered structure are same, the resonant wavelength is not same for all the rod shapes owing to unique filling fraction. The different rod shape in a structure gives unique filling fraction in turn resonant wavelength. The space filled by circular, hexagonal and square rods is increased linearly (11.775×10^{-12} sq.m, 12.975×10^{-12} sq.m and 15×10^{-12} sq.m) whose corresponding resonant wavelength is 1497 nm, 1507 nm and 1523 nm respectively. It is concluded that there is 1 nm wavelength shift at resonant wavelength is observed for increasing filling fraction of 0.1233×10^{-12} sq.m which describes that the resonant wavelength depends on the filling fraction. The change in filling fraction can be done by increasing the rod radius or changing the shape of the rods.

In general, the dropping efficiency is defined as the output power reached at port D at resonance. Similarly, the power reached at port B is subtracted by 100 is termed as coupling efficiency. The Q factor is calculated as $\lambda/\Delta\lambda$ and passband width is the width of the band at resonance which is taken at Full Width Half Maximum (FWHM) point.

In addition, the resonant wavelength can also be shifted by varying the dielectric constant and lattice

constant of the structure. While increasing the aforementioned parameters the resonant wavelength shifts linearly into the longer wavelength and vice-versa. By choosing appropriate values for these parameters, it is possible to add or drop any one of the desired channels of ITU-T 694.2 CWDM [27] systems whose specified channel spacing and passband width are 20 nm and 13 nm \pm 1.5 nm, respectively. The resonant wavelength, coupling and dropping efficiencies, passband width and Q factor of square, circular and hexagonal rods based ADF without and with scatterer rods are listed in the above Table 3.

Table 3. Resonant wavelength, coupling and dropping efficiencies, passband width and Q factor of square, circular and hexagonal rods.

Rod Shape		RW (nm)	CE (%)	DE (%)	PW (nm)	Q factor
Square	a*	1523	95	75	19	80.15
	b*	1520	98	96	16	95
Circular	a*	1497	98	80	15	99.8
	b*	1494	100	100	12	124.5
Hexagonal	a*	1507	98	90	17	88.6
	b*	1504	100	100	14	107.4

a* \rightarrow without scatterer rods; b* \rightarrow with scatterer rods
 CE \rightarrow Coupling efficiency; DE \rightarrow Dropping efficiency
 RW \rightarrow Resonant wavelength; PW \rightarrow Passband width

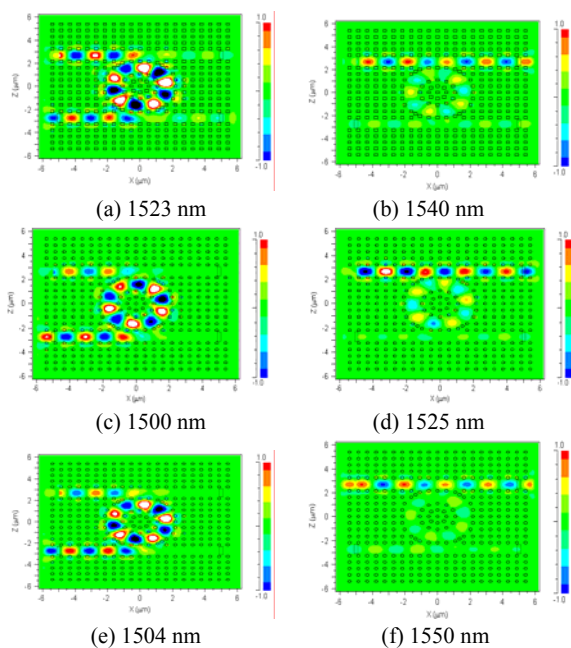


Fig. 12. Electric field pattern of pass and stop region of square rods (a) & (b), circular rods (c) & (d), and hexagonal rods (e) & (f).

The Figs. 12 (a) and (b), (c) and (d), and, (e) and (f) depict the electric field pattern of pass region and stop region of square, circular and hexagonal rods based ADF with scatterer rods. At resonant wavelength the electric

field of the bus waveguide is fully coupled into the ring and reached into one of its output ports, whereas at 'off' resonance the signal directly reaches the transmission terminal without coupling the ring resonator.

5. Conclusions

The impacts of rod shape and filling fraction are numerically analyzed by designing two dimensional photonic crystal circular ring resonator based Add Drop Filter. Its performance with respect to the resonant wavelength, coupling efficiency, dropping efficiency, passband width and Q factor is compared for all the structures without and with scatterer rods. The resonant wavelength of the filter is not same for all the rod shape due to unique filling fraction. The overall filling fraction and resonant wavelength of a square, circular and hexagonal rod based structures are 15×10^{-12} sq.m, 11.775×10^{-12} sq.m and 12.975×10^{-12} sq.m and 1523 nm, 1497 nm and 1507 nm, respectively. It is concluded that there is 1 nm wavelength shift is observed while increasing the overall filling fraction by 0.1233×10^{-12} sq.m. Also, it is observed that filling fraction linearly depends on the resonant wavelength. Close to, 100% of coupling and dropping efficiencies are observed for circular and hexagonal rod based ADF with scatterer rods whose Q factor is 124.5 and 107.42, respectively. Hence, the authors recommend both circular and hexagonal rod geometry for the design of PCRR based ADF to get better results.

Appendix

A1. Effect of Gap map

In this appendix, the profile of the gap map is simulated by varying delta (dielectric constant difference), width (for square rod)/radius (for circular and hexagonal rods) of the rod and period (lattice constant) for square, circular and hexagonal rods as shown in Figs. A1, A2 and A3. Generally, the gap map plays a crucial role in determining geometrical parameters to design the optical devices. It also imparts respective impact of TE/TM PBG for varying various structural parameters. Here, the blue region represents the TE PBG whereas red region illustrates TM PBG and green region depicts complete PBG. The complete PBG is defined as the range of PBG present for both TE and TM.

The values of the structural parameters such as delta (2.46), rod radius (0.1 μ m), width (0.2) and period (540 nm) used for the design of this filter are derived from the gap map. The value of delta, lattice constant, and the number of rods in the structure is kept same in all three filters to maintain the footprint of the device.

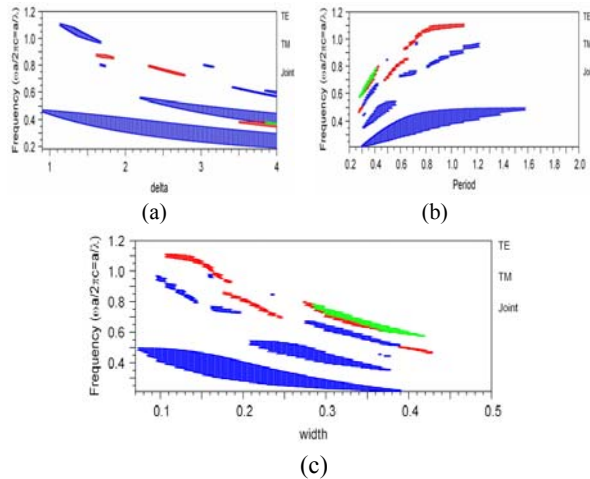


Fig. A1. Effect of gap map for square rods (a) delta (b) period and (c) width.

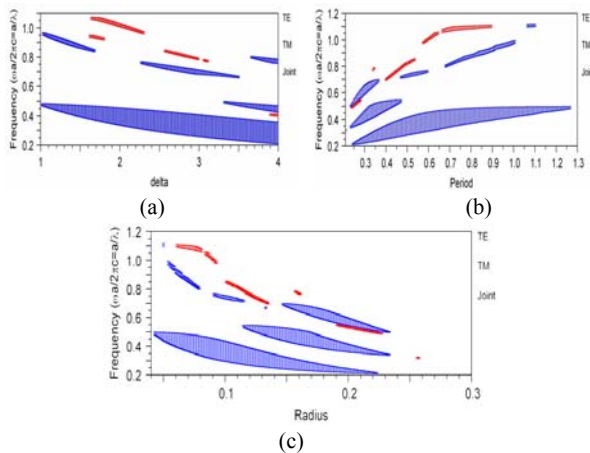


Fig. A2. Effect of gap map for circular rods (a) delta (b) period and (c) width.

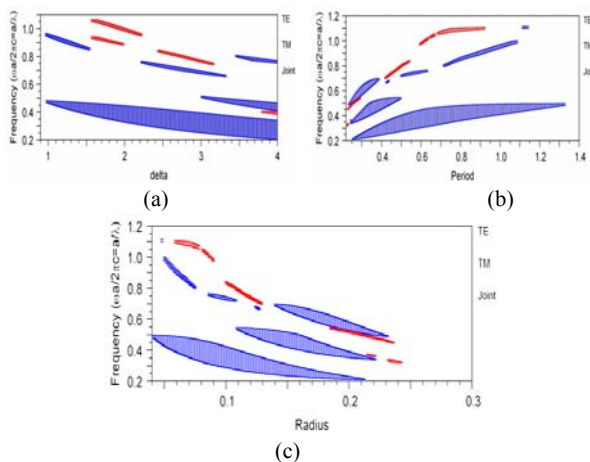


Fig. A3. Effect of gap map for hexagonal rods (a) delta (b) period and (c) width.

Finally, it is also noted that while increasing the value of delta, width and radius of the rod, the PBG region shifts into longer wavelength region and the PBG shifts into shorter wavelength region while increasing the value of period or lattice constant. In addition, the TE PBG increases linearly with delta, however, it increases till some point afterwards starts to decrease for period, width and radius of the rod.

References

- [1] E. Yablonovitch., Phys. Rev. Lett. **58**(20), 2059 (1987).
- [2] S. John, Phys. Rev. Lett. **58**(23), 2486 (1987).
- [3] Dan Sadot, Efraim Boimvich, IEEE Communication magazine, 50 (1998).
- [4] J. D. Joannopoulos, R. D. Meade, J. N. Winn, Princeton, NJ: Princeton university press, (1995).
- [5] J. D. Joannopoulos, P. R. Villeneuve, S. Fan, Nature **386**, 143 (1997).
- [6] A. Ghaffari, F. Monifi, M. Djavid, M. S. Abrishamian, Journal of Applied Science **8**(8), 1416 (2008).
- [7] G. Manzacca, D. Paciotti, A. Marchese, M. S. Moreolo, G. Cincotti, Photonics and Nanostructures-Fundamentals and Applications **5**(4), 164 (2007).
- [8] A. Ghaffari, F. Monifi, M. Djavid, M. S. Abrishamian, Optics Communications **281**(15-16), 4028 (2008).
- [9] V. Zabelin, L. A. Dunbar, N. Le Thomas, R. Houdre, M. V. Kotlyar, L. O'Faolain, T. F. Krauss Optics Letters **32**(5), 530 (2007).
- [10] Tien-Tsornq shih, Yaw-Dong Wu, Jian-Jang Lee, IEEE Pho. Tech. Lett. **21**(1), 18 (2009).
- [11] Qiong Wang, Yiping Cui, Hiayu Zhang, Changchun Yan, Lingling Zhang, Optik Optics **121**(8), 684 (2010).
- [12] M. K. Moghaddam, A. R. Attari, M. M. Mirsalehi, Photonics and Nanostructures-Fundamentals and Applications **8**(1), 47 (2010).
- [13] S. Robinson, R. Nakkeeran, SPIE Journal of Nanophotonics **5**, (posted 11th July 2011, in press) [DOI:10.1117/1.3615987].
- [14] M. Djavid, A. Ghaffari, F. Monifi, M. S. Abrishamian, Journal of Applied Science **8**(10), 1891 (2008).
- [15] S. Robinson, R. Nakkeeran, Optik Optics (posted 13th 2011, in press) [DOI: 10.1016/j.ijleo.2011.05.004].
- [16] S. Fan, P. R. Villeneuve, J. D. Joannopoulos, H. A. Haus, Opti. Express **3**(1), 4 (1998).
- [17] Chun-Chih Wang, Lien-Wen Chen, "Physica B **405**(4), 1210 (2010).
- [18] M. Djavid, A. Ghaffari, F. Monifi, M. S. Abrishamian, Physica E **40**(10), 3151 (2008).
- [19] B. S. Darki, N. Granpayesh, Optics Communications **283**(20), 4099 (2010).
- [20] Z. Qiang, W. Zhou, Richard A. Soref, Opti. Express **15**(4), 1823 (2007).
- [21] Juan Jose Vegas Olmos, Masatoshi Tokushima,

- Kenichi Kitayam, *Journal of Selected Topics in Quantum Electronics* **16**(1), 332 (2010).
- [22] M. Djavid, A. Ghaffari, F. Monifi, M. S. Abrishamian, *Journal of Applied Sciences* **8**(11), 2178 (2008).
- [23] Trong Thi mai, Fu-Li Hsiao, Chengkuo Lee, Wenfeng Xiang, Chii-Chang Chen, W. K. Choi, *Sensors and Actuators A: Physical* **165**(1), 16 (2011).
- [24] S. Robinson, R. Nakkeeran, *Springer Optoelectronics Letters* **7**(3), 164 (2011).
- [25] A. Lavrinenko, P. I. Borel, L. H. Frandsen, M. Thorhauge, A. Harpoth, M. Kristensen, T. Niemi, H. M. H. Chong, *Opti. Express* **12**(2), 234 (2004).
- [26] C. Manolatou, M. J. Khan, S. Fan, P. R. Vileneuve, H. A. Haus, J. D. Joannopoulos, *Journal of Quantum Electronics* **35**(9), 1322 (1999).
- [27] ITU-T Recommendation G 694.2, Spectral grids for WDM applications: CWDM wavelength grid.

*Corresponding author: mail2robinson@pec.edu